Double-Channel Photoionization Followed by Geminate Charge Recombination/Separation

ARTICLE *in* THE JOURNAL OF PHYSICAL CHEMISTRY A · OCTOBER 2009

Impact Factor: 2.69 · DOI: 10.1021/jp901863t · Source: PubMed

2 AUTHORS:

Serguei Feskov
Volgograd State University
19 PUBLICATIONS **172** CITATIONS
SEE PROFILE

Anatoly Israel Burshtein
Weizmann Institute of Science
216 PUBLICATIONS **3,128** CITATIONS
SEE PROFILE

Double-Channel Photoionization Followed by Geminate Charge Recombination/Separation

Serguei V. Feskov*,† and Anatoly I. Burshtein*,‡

Department of Physics, Volgograd State University, University Avenue, 100, Volgograd, 400062, Russia, and Weizmann Institute of Science, Rehovot 76100, Israel

Received: February 28, 2009; Revised Manuscript Received: September 7, 2009

The photoionization of perylene by tetracyanoethylene (TCNE) in liquid solutions is reconsidered within the corrected energy scheme for a double channel electron transfer: to the ground and excited states of the produced ion pair. The complex space dependence of a total (double channel) rate of multiphonon transfer is specified and compared to the recently proposed monoexponential model. The fitting of the forward electron transfer (ionization) is essentially improved, and the real electron coupling and tunneling parameters are firmly established. The same has been done for the geminate recombination/separation kinetics, accounting theoretically for the hot recombination experienced by 2/3 of the initially produced ion pairs. Only 1/3 of them is left for subsequent thermal recombination and even less are left for their separation into free ions. The yields of the latter, strongly dependent on the initial concentration of TCNE, are brought into reasonable coincidence with the theoretical predictions by a renormalization of the empirically calibrated ion densities especially at large concentrations. Altogether, this is a precedent spin-less treatment of photoionization well-fitted to the experimental data at all times (from the excitation until charge separation), with a single set of varying parameters.

I. Introduction

The excitation quenching by electron transfer in solution is a distant reaction proceeding with the rate $W_I(r)$ at any distance r between the reactants

$$\begin{matrix} D^* \\ \downarrow\tau_D \end{matrix} + A \overset{W_I}{\Rightarrow} D^+ + A^- \qquad (1.1)$$

In conventional Markovian theory it proceeds exponentially

$$N^* = [D^*] = N^*(0)\exp(-t/\tau_D - ck_it) \qquad (1.2)$$

where $c = [A]$ is the quencher concentration. According to differential encounter theory (DET),[1,2] the rate constant

$$k_i = 4\pi R_Q D \qquad (1.3)$$

is proportional to encounter diffusion coefficient D and the effective quenching radius $R_Q(D)$ that was first specified long ago for the exponential model of tunneling rate[3]

$$W = W_c e^{-2(r-\sigma)/l} \qquad (1.4)$$

Here, σ is a contact distance where the rate (W_c) is maximal, while l is the effective tunneling length. Unfortunately, the very first application of such a Markovian DET to really studied quenching of the pheophytin a fluorescence by toluquinone showed that l is greatly overestimated.[4]

This paradox was resolved in a subsequent study of the similar phenomenon but with much better resolution.[5] It was proved that Markovian asymptotics eq 1.2 is never reached in the available time range. Only general non-Markovian quenching kinetics is seen which is nonexponential and precedes the exponential one:

$$P = N^*/N^*(0)\exp(-t/\tau_D) = \exp(-c\int_0^t k_I(t')dt') \qquad (1.5)$$

The long time behavior of the non-Markovian time dependent rate constant

$$k_I(t) = 4\pi R_Q D\left(1 + \sqrt{\frac{R_Q^2}{\pi Dt}}\right) \text{ at } t \to \infty \qquad (1.6)$$

was detected. From this expression where the second term dominates in available time range the right value of R_Q was specified, and correct value of l was extracted from its diffusional dependence.

In a later work,[6] the experimental study of quenching was extended even for shorter times up to the static quenching following immediately after the pumping pulse. The exponential static quenching starts with a rate constant

$$k_I(0) = \int W_I(r)d^3r = k_0 \qquad (1.7)$$

which is a kinetic rate constant equal to the first moment of $W_I(r)$. Getting this constant from the initial quenching kinetics, one can fit to it the ionization rate getting its main parameters and keeping diffusion for fitting the rest of excitation decay. The chemical system investigated here consists of perylene (Pe)

* Corresponding author.
† Volgograd State University.
‡ Weizmann Institute of Science.

10.1021/jp901863t CCC: $40.75
Published on Web 10/23/2009

in the first singlet excited state as electron donor in the presence of tetracyanoethylene (TCNE) in acetonitrile.[7] This is the most exergonic system allowing the electron transfer not only in the ground state ion pair but also in its excited states. It was shown that at least one of them should be accounted for turning ionization into double-channel reaction. Such a kinetics was well-fitted, assuming that the forward electron transfer proceeds not only to the ground state of the ion pair but also to the lowest electronically excited state of it:

$$\begin{array}{ccccc} & & & & [D^+...A^-]^* \\ & & & W^* \nearrow & \\ D^* & + & A & & \\ \downarrow \tau_D & & & W_0 \searrow & \\ & & & & [D^+...A^-] \end{array} \qquad (1.8)$$

The subsequent backward electron transfer (ion recombination) in such an obtained ion pairs $[D^+ \cdots A^-]$ and $[D^+ \cdots A^-]^*$ accompanied by diffusional charge separation is fitted in the next article,[8] although not as well. The theory explains the low yield of free ions due to their hot recombination but predicts much slower accumulation of them than it is in reality and a bit longer dissipation leading to a smaller free ion quantum yield. Interestingly, the latter depends actually on the quencher concentration c (see Table 3 in ref 7) but this phenomenon was left unexplained. Here, we are going to eliminate all of these weaknesses starting from the interpretation of the ionization kinetics.

The theory will be revised here from the very beginning using the new contact value for the reorganization energy

$$\lambda_c = 0.86\text{eV} \qquad (1.9)$$

instead of the previously chosen (rather arbitrarily) $\lambda_c = 1.15$ eV.[6,8] As a matter of fact, λ_c is the main important parameter determining the reorganization energy at any reactant separation,

$$\lambda(r) = \lambda_c\left[2 - \frac{\sigma}{r}\right]$$

The latter fixes the splitting of the reactant and product parabolic terms, which is equal to 2λ at any given r (Figure 1). The contact reorganization energy is usually estimated from the Marcus theory of electron transfer in polar media:

$$\lambda_c = \left(\frac{1}{\varepsilon_0} - \frac{1}{\varepsilon}\right)e^2\left[\frac{1}{2r_D} + \frac{1}{2r_A} - \frac{1}{\sigma}\right]$$

where ε and ε_0 are the static and optical dielectric permittivities of the solvent. In acetonitrile, their values are known, $\varepsilon = 37.5$, $\varepsilon_0 = 1.8$, while the effective contact distance in Per/TCNE pair is taken to be $\sigma = r_D + r_A \approx 6$ Å. The accuracy of this choice is not crucial because the main electron transfer in such a system being under diffusion control[6] occurs far away from contact, at quenching sphere of radius $R_Q \gg \sigma$, and almost nothing happens deep inside it, near the contact. On the contrary, the contact reorganization energy λ_c, as well as the free energies of the ground and excited state ions production, $\Delta G_0 = -2.14$ eV and $\Delta G^* = -0.6$ eV, and recombination to the ground state of the reactants, $\Delta G_R = -0.69$ eV, play an important role. They determine all of the level crossings and the energy distances between them (Figure 1). This ensured that the right specification of λ_c is very important. Here, it is carried out spectroscopically.

The initial excitation of perylene in the experiment[7] was performed at 400 nm. The energy of the $D \rightarrow D^*$ transition is $\Delta E^* = -\Delta G_I - \Delta G_R = 2.83$ eV (~439 nm) while the energy of the straightforward excitation to the ground state ion pair is

$$\Delta E = \lambda - \Delta G_R \qquad (1.10)$$

The frequency of the charge transfer band (~800 nm)[7] in Per/TCNE complexes allows us to estimate the contact value $\Delta E(\sigma) = 1.55$ eV directly from experiment and, thus, calculate λ_c (eq 1.9) using eq 1.10. Being smaller than previously used, it reduces the horizontal splitting of the parabolas in Figure 1A.

This makes the current consideration qualitatively different from the previous one. The electron transfer to the ground state ion pair becomes more activated and weaker, whereas the competing transfer between excited states becomes almost activationless and therefore more efficient. The former proceeds in the inverted region, with the bell shaped rate $W_0(r)$ shifted

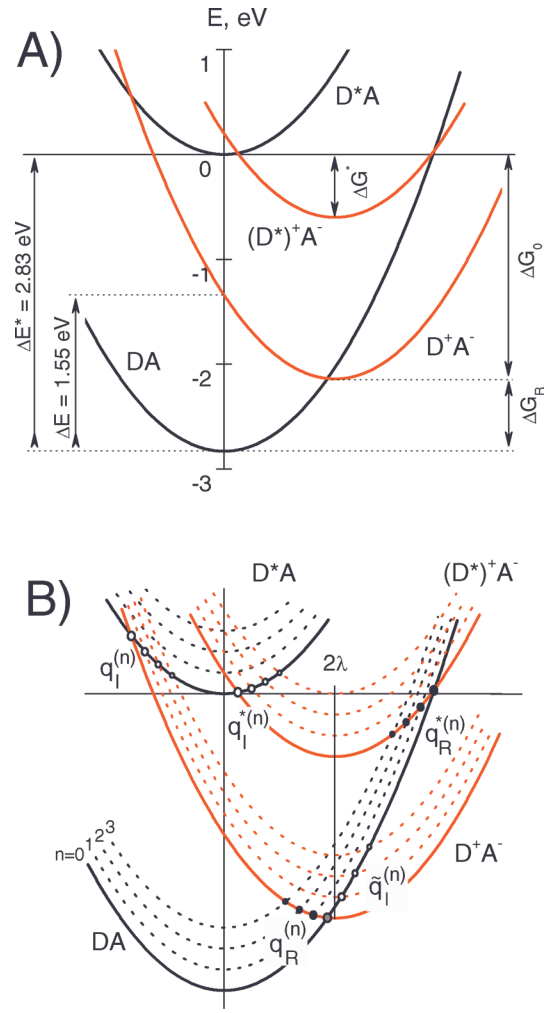

Figure 1. (A) Electron transfer energy scheme of the Per/TCNE system. The left parabolas represent the reactants while the ion pair states are given by the right ones. (B) The same scheme for the phonon-assisted electron transfer via crossing points representing the forward (○) and backward (●) reaction.

out of contact, while the rate of the latter, $W^*(r)$, is quasi-exponential acting only near the contact (see Figure 10 in ref 6).

Due to hot recombination, following initial photoexcitation and electron transfer, only a small remaining fraction of the survived radical ion pairs (RIPs) is subjected to subsequent thermal recombination, accelerated by the encounter diffusion of the counterions.[8] The latter proceeds with the diffusion coefficient $\tilde{D}$ which is identified with its analog for the neutral particles D. Found here from the best fit of the DET[1] to the transfer kinetics, it was shown to be

$$D = 2.6 \times 10^{-5}\ \mathrm{cm}^2/\mathrm{s} \tag{1.11}$$

How sensitive is this choice to the variation of D is shown in Figure 6A. The result is just a bit smaller than the previously obtained value $D = 3.05 \times 10^5\ \mathrm{cm}^2/\mathrm{s}$.[6,8]

The outline of this paper is as follows.

In section II, we will present the theory revising the forward electron transfer kinetics in the frame of the new energy scheme. The rates of phonon-assisted double channel electron transfer, limited by dynamic solvent effect (DSE), will be specified as functions of the free energies of ionization and reactants separation. Then, the initial static ionization convoluted with initial pumping pulse was fitted to the shortest experimental decay to get not a single k_0 but two rate moments: $k_0 = Wd^3r$ and $k_2 = W^2d^3r$. By fitting to them the above rates, the main electronic coupling in competing ionization channels as well as an electron−phonon constant S (common for both) were specified. The subsequent diffusion accelerated ionization was fitted separately varying only diffusion coefficient, and the long time decay with the time dependent constant (eq 1.6) was reproduced at the right choice of D (eq 1.11). After the space dependence of both ionization rates and all of the fitting parameters were specified, the theory was compared with an alternative one using the popular exponential model of a single ionization rate. Finally, it is used for the calculation of the initial distribution of ion pairs preceding their geminate recombination.

In section III, the backward electron transfer during ion recombination and separation is treated within unified theory (UT). This theory developed simultaneously in two pioneering works[9,10] and reviewed in ref 1 is actually an extension of DET allowing to trace the farther evolution of ion pairs produced by preceding ionization. The separation and recombination of these pairs (RIPs) crucially depends on their initial distribution (separation) prepared by ionization. UT describes both the initial accumulation of RIPs and their subsequent dissipation. It states that the initial ion accumulation should be linear in time and concentration, but in present experiment, the linearity in concentration is broken. It can be restored if the actual fraction of the ion pairs accumulated at different quencher concentrations is corrected, being multiplied on the factor $\gamma(c)$ which is larger than 1 at higher c. This may be the result of an additional (straightforward) light excitation of RIPs that we ignored here.

The same renormalization is used here for fitting the subsequent charge dissipation within the extended UT employed the first time. The extension implies that the contribution of hot recombination preceding the thermal recombination is calculated analytically, assuming that the motion along the reaction coordinates is rather fast (instantaneous). By fitting the subsequent thermal recombination, all of the parameters of the backward transfer are specified as well and used for the restoration of the rate of ion recombination after thermalization. The latter is used for the estimation of the free ion recombination constant that can be verified by investigation of ion recombination in the bulk, following the geminate one.

The discussion of the results are presented in Conclusions.

II. Double-Channel Bimolecular Ionization

The distant electron transfer, modulated by the encounter diffusion of the reactants, is well-described by the differential encounter theory (DET). The measured intensity of perylene fluorescence is proportional to the number of fluorescent molecules $N^*(t)$:

$$N^*(t) = N_0 \int_0^t f(t')R(t - t')\,\mathrm{d}t' \tag{2.1}$$

where N_0 is the initial number of excited molecules. This is actually a convolution of their survival probability $R(t)$ and the quantity $N_0 f(t)$ which is proportional to the instrument response function (IRF)

$$f(t) = \frac{1}{\sqrt{2\pi}\Delta} \exp\left(-\frac{(t - t_c)^2}{2\Delta^2}\right)$$

The full width at half-maximum of IRF, $2(2\ \ln\ 2\Delta)^{1/2}$, is known to be 200 fs, while the IRF center, $t_c = 1.05$ ps, is obtained here from the fitting to the available experimental data.

It was shown in ref 6 that the fluorescent state is populated by the vibrational relaxation from the primary excited vibronic state to the lowest one. The population of the latter is actually a convolution of its vibrational pumping, proceeding exponentially with the time τ_v and the system response to the instantaneous excitation $N(t)$:

$$R(t) = \int_0^t N(t - t')\, e^{-t'/\tau_v}\,\mathrm{d}t'/\tau_v \tag{2.2}$$

The fraction of excitations which escaped ionization up to the time t, $N(t)$, obeys the conventional equation of DET:[1,2,11]

$$\dot{N} = -ck_I(t)N - N/\tau_D\,,\quad N(0) = 1 \tag{2.3}$$

For our system (perylene in acetonitrile), the excitation lifetime τ_D is known to be $\tau_D = 4.34$ ns.

Here and below, the time dependent rate constant of the forward electron transfer (ionization) is

$$k_I(t) = \int W_I(r)n(r,t)d^3r \tag{2.4}$$

The pair correlation function $n(r,t)$ takes into account that the remote transfer running with rate $W_I(r)$ is accelerated by the encounter diffusion, represented by the operator $\hat{L}$:

$$\dot{n} = -W_I(r)n + \hat{L}n \tag{2.5}$$

If there is no inter-reactant interaction, then the diffusional operator $\hat{L} = D\Delta$, while the initial and the boundary conditions to eq 2.5 take the following form:

$$n(r,0) = 1 \quad \text{and} \quad \left.\frac{\partial n}{\partial r}\right|_{r=\sigma} = 0 \tag{2.6}$$

The double channel electron transfer rate

$$W_I(r) = W_0(r) + W^*(r) \tag{2.7}$$

is an input data for the theory: the ground state ion pair appears with the rate $W_0(r)$, while the same pair in its excited state is produced with the rate $W^*(r)$.

A. Dynamic Solvent Effect. The general expression for the phonon-less electron transfer rate at given exergonicity ΔG has the well-established form[1]

$$W(r) = \frac{U(r)}{1 + U(r)\tau} e^{-(\Delta G+\lambda)^2/4\lambda T} \tag{2.8}$$

It is constituted from the Arrhenius factor specified by Marcus[12] and the pre-exponent accounting for the dynamic solvent effect (DSE).[13−15] The latter establishes the upper limit for W

$$W \le \frac{1}{\tau} e^{-(\Delta G+\lambda)^2/4\lambda T}$$

which is the rate of reaching the crossing point from the bottom of the well (by diffusional motion along the reaction coordinate). If τ is short enough, then the reaction proceeds straight from the equilibrated (thermal) state, with the rate specified from the perturbation theory in the second order approximation with respect to the electronic coupling V,

$$U(r) = \frac{V^2}{\hbar} \exp\left(-\frac{2(r-\sigma)}{L}\right) \frac{\sqrt{\pi}}{\sqrt{\lambda T}} \tag{2.9}$$

where L is the tunneling length. For the Per/TCNE system, it was found to be[6,8]

$$L = 1.24\ \text{Å}$$

and the same value will be used in this article.

It is known[13] that the DSE rate for the phonon-less system (Figure 1A) is

$$\frac{1}{\tau} = \frac{1}{4\tau_L}\sqrt{\frac{\lambda}{\pi T}} \tag{2.10}$$

Here, τ_L is the longitudinal relaxation time of the solvent polarization which assists the electron transfer. In fact, this expression is just an interpolation of a much more complex free energy dependence

$$\frac{\tau_L}{\tau} = \Phi\left(\frac{\Delta G}{\lambda}, \frac{\lambda}{T}\right) \tag{2.11}$$

Such a dependence first specified by Zusman[13] was recognized to be incorrect near $-\Delta G = \lambda$, and another one was proposed instead.[16] The true dependence was specified numerically (for $\lambda = 1$ eV and room temperature) in our recent work,[17] and its analog for the new $\lambda = 0.86$ eV is also presented in Figure 2. The particular values for the two competing channels could be taken from $\Phi(\Delta G)$ for one ($\Delta G_0 = -2.14$ eV) or another ($\Delta G^* = -0.6$ eV) arguments corresponding to their free energies.

B. Phonon-Assisted Electron Transfer Rates. The situation is more complex when the electron transfer is assisted by intramolecular quantum mode (Figure 1B) so that the ion pair appears in one of the vibrational states of this mode: $n = 0, 1, \ldots$. Neglecting DSE, one can specify the total rate of such a multiphonon transfer between the electronic levels as a sum of the particular channel rates weighted with the particle density in the crossing points:

$$W(r) = \int \sum_n \frac{2\pi V^2(r)}{\hbar} \frac{e^{-S} S^n}{n!} \delta(q - q^{(n)}(r)) \varphi_0(q) dq \tag{2.12}$$

where the thermal distribution of excitations is

$$\varphi_0(q) = (4\pi\lambda T)^{-1/2} \exp\left(-\frac{q^2}{4\lambda T}\right)$$

$$\text{and} \quad q^{(n)} = \lambda + \Delta G + n\hbar\omega$$

Here, ω is the vibrational frequency and $S = \lambda_q/\hbar\omega$, where λ_q is the reorganization energy of the quantum vibration. As in our previous paper, we fix $\hbar\omega = 0.1$ eV.

Assuming that the ion density is always thermalized by fast vibronic relaxation and accounting for the DSE in both acting channels, we have for the corresponding ionization rates:[6]

$$W_0(r) = \sum_0^\infty \frac{U_0(r) e^{-S} S^n}{n! + U_0(r)\tau_0 e^{-S} S^n} \exp\left[-\frac{(\Delta G_0 + \lambda + \hbar\omega n)^2}{4\lambda T}\right] \tag{2.13a}$$

$$W^*(r) = \sum_0^\infty \frac{U^*(r) e^{-S} S^n}{n! + U^*(r)\tau^* e^{-S} S^n} \exp\left[-\frac{(\Delta G^* + \lambda + \hbar\omega n)^2}{4\lambda T}\right] \tag{2.13b}$$

According to eq 2.9, $U_0 \propto V_0^2$ while $U^* \propto (V^*)^2$. In eq 2.13b, only V_0 and V^* together with S will be used later as the varying parameters, keeping $\tau_0 = \tau(\Delta G_0)$ and $\tau^* = \tau(\Delta G^*)$.

Generally speaking, the vibronic states of ion products are unstable and relax to the lower ones with the rate of vibrational relaxation, $1/\tau_v$, that we assume to be the fastest one. In such a

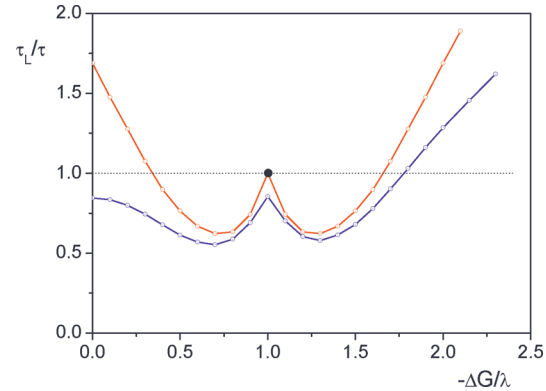

Figure 2. Free energy dependence of τ_L/τ calculated numerically at $\lambda = 0.86eV$ (solid lines). The blue and red lines correspond to the reversible and irreversible transfer, respectively. The symbol ● points to the result of ref 18 .

case, the electron transfer is irreversible, and the function 2.11 is a bit different. In fact, the irreversible DSE was first explored analytically but only for a single point, $\Delta G = -\lambda$, where the electron transfer is activationless and nonexponential.[18] However, the long time electron transfer proceeds always exponentially with a rate $1/\tau$ whose free energy dependence is calculated here numerically and shown in Figure 2. Taking $\tau_L = 0.5$ ps in acetonitrile, one obtains the following τ (Table 1) for all crossing points for vibrationless ionization and recombination:

TABLE 1

	$q_I^{(n)}$	$q_I^{*(n)}$	$q_R^{(n)}$	$q_R^{*(n)}$
ΔG, eV	−2.14	−0.60	−0.69	−2.23
τ_{rev}, ps	0.268	0.905	0.852	0.266
τ_{irr}, ps	0.188	0.804	0.791	0.186

For simplicity, the same values of τ will be taken for all of the vibrational repetitions of the crossing points ignoring the difference in their activation energies. Since in the most of them the level accepting the electron is vibrationally unstable, we preferred to use everywhere an appropriate τ_{irr} from Table 1.

C. Fitting to the Initial Quasi-Static Decay. Immediately after excitation but before the partners (D^* and A) start to move, the excitations are subjected to the distant static decay. During this short interval, one can set $\hat{L} = 0$ and, integrating eq 2.5, use the result, $n(r,t) = e^{-W_I(r)t}$, in eq 2.4 to specify the static rate constant:

$$k_1(t) = \int W_I(r) e^{-W_I(r)t} d^3r \approx k_0 - k_2 t + \cdots \tag{2.14}$$

where the kinetic rate constant

$$k_0 = k_I(0) = \langle W_I \rangle = \int W_I(r) d^3r \quad \text{and} \quad k_2 = \langle W_I^2 \rangle = \int W_I^2(r) d^3r \tag{2.15}$$

are the first two moments of the transfer rate.

At the very beginning, the excitation dissipation and the corresponding ion pair accumulation proceed with the same kinetic rate, $k_I(t) = k_0 = \text{const}$, and obey the following set of equations:

$$\dot{N}^* = N_0 \int_0^t e^{-(t-t')/\tau_v} f(t') dt'/\tau_v - c k_0 N^* - \frac{N^*}{\tau_D} \tag{2.16a}$$

$$\dot{N}_\pm = N^* c k_0 \tag{2.16b}$$

where $k_0 = k_I(0)$, while $N_\pm$ is the number of accumulated ion pairs. After a short pulse and fast vibrational relaxation (but before the excitation decay), the total number of excitations accumulated in the lowest vibrational sublevel is

$$N^*(\tau_v) = N_0 \int_0^\infty dt \int_0^t e^{-(t-t')/\tau_v} \delta(t') dt'/\tau_v = N_0 \tag{2.17}$$

Substituting this result into eq 2.16b instead of N^*, we conclude that after all of the excitations have been accumulated in their ground state the share of ion pairs grows linearly with time:

$$P = \frac{N_\pm}{N_0} = c k_0 t \tag{2.18}$$

The growing of the ionic population becomes slower when the recombination starts. Later on, when the recombination exceeds the ionization, the accumulation of ion pairs gives way to their dissipation considered below.

Using the short time approximation to static rate constant (eq 2.14) when integrating eq 2.3, we get:

$$N(t) = e^{-\int_0^t k_I(t') dt' - t/\tau_D} \approx e^{-c[k_0 t - k_2 t^2/2] - t/\tau_D} \tag{2.19}$$

With this result substituted into eq 2.2, one accounts for the system response on vibrational pumping in the quasi-static approximation:

$$R(t) = \int_0^t e^{-c[k_0(t-t') - k_2(t-t'^2/2] - (t-t')/\tau_D} e^{-t'/\tau_v} dt'/\tau_v \tag{2.20}$$

Substituting this R into the convolution 2.1, we have to fit the real data having only three varying parameters, k_0, k_2, and τ_v. Nonetheless, the quality of the fitting shown in Figure 3 is quite reasonable, provided that the moments of the transfer rate are

$$k_0 = 530\,\text{Å}^3/\text{ps} \quad \text{and} \quad k_2 = 70\,\text{Å}^3/\text{ps}^2 \tag{2.21}$$

These parameters are the same for all curves in Figure 3, while τ_v varies with c within the interval $\tau_v = 0.14 \div 0.21$ ps.

The validity region of the power time expansion (eq 2.14) is restricted by the evident inequality

$$t \ll k_0/k_2 = 7.6\ \text{ps}$$

This time interval is obviously wider than that where initial quasi-static kinetics was studied for specification k_0 and k_2 (see Figure 3).

Getting true k_0 and k_2, one can set strict limitations on the three microscopic quantities, V_0, V^*, and S, according to eqs 2.15 and 2.13a. This can be done in two steps. First, we find the family of curves $V^*(V_0)$ which correspond to different S with $k_0(V_0,V^*,S) = 530$ Å^2/ps keeping constant (Figure 4A). Then, the variation of k_2 along these curves is calculated from its definition (eq 2.15) and the contour map $k_2(V_0,V^*)$ is constructed (Figure 4B). One can easily see from this plot that the k_2 value closest to that estimated in eq 2.21 can be obtained only near the lowest curve.

This allows us to specify immediately the best fit microscopic parameters for the ground and the excited state ionization channels which are indicated by symbol ⊗ in Figure 4A,B.

$$V_0 = 0.15\ \text{eV} \quad V^* = 0.01\ \text{eV} \quad S = 2.5 \tag{2.22}$$

The relative contribution of the two channels given by the ratio V^*/V_0 is 0.07 against 1.12 in our previous paper.[6] However, we will show later that the production of the excited ion pairs

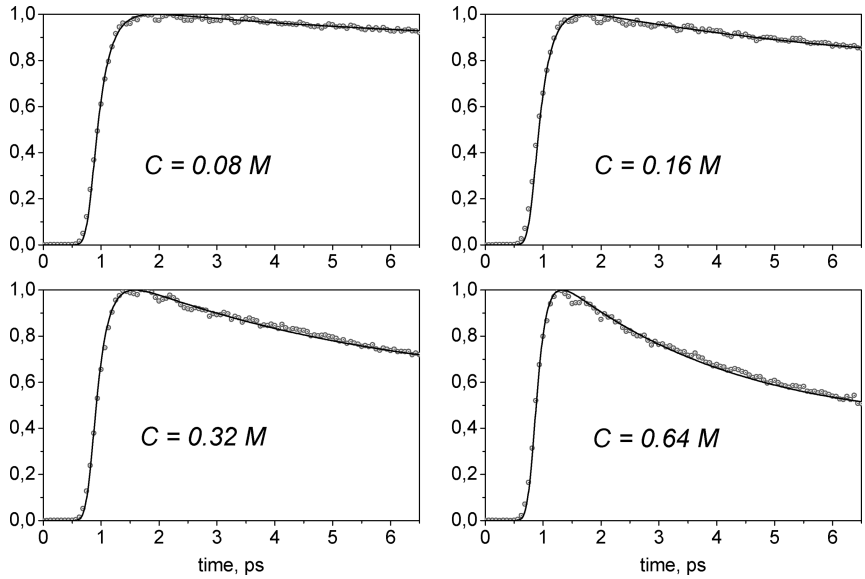

Figure 3. Fitting the initial accumulation and decay of the fluorescent state at different quencher concentrations.

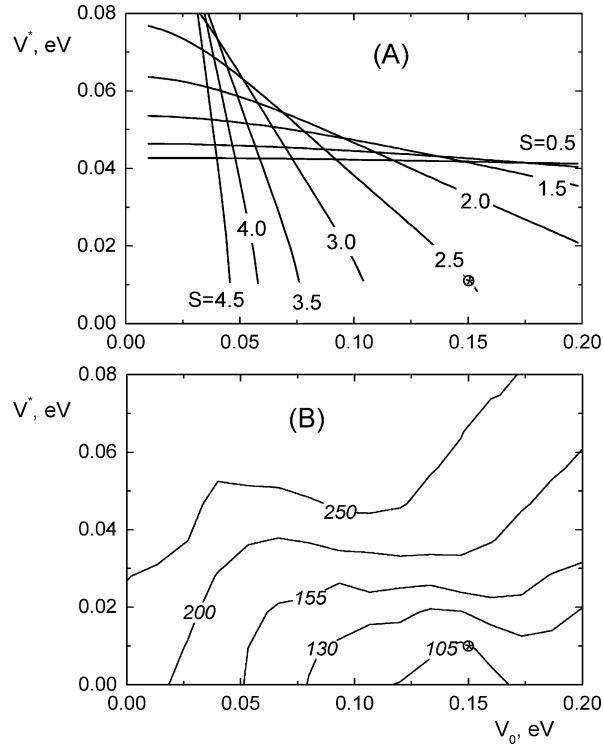

Figure 4. (A) Family of curves satisfying the condition $k_0 = \langle W_I \rangle = 530$ Å^3/ps at different S. (B) Contour map of k_2 values calculated along the curves shown in A. Symbol star-in-circle on both plots shows the point with k_0 and k_2 closest to those established for Per/TCNE system in eq 2.21. This point coordinates provide the microscopic ionization parameters V, V^*, S (eq 2.22).

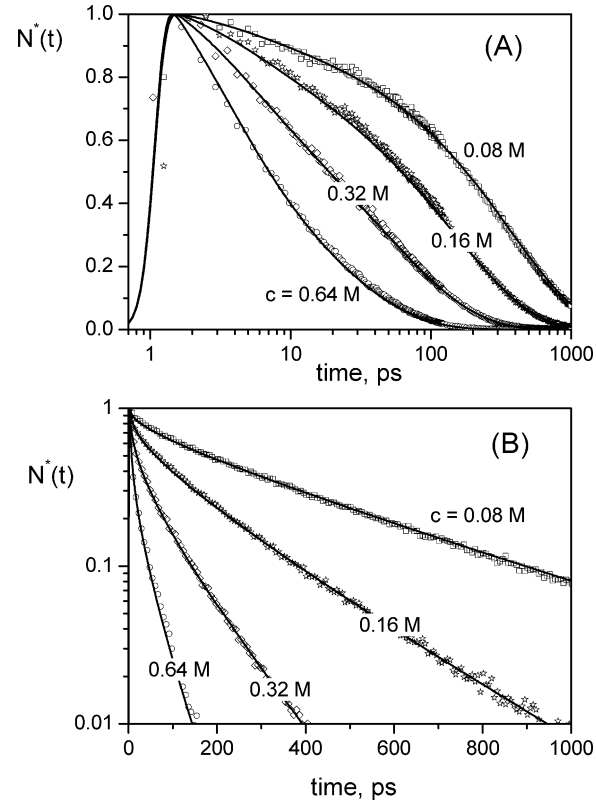

Figure 5. (A) Fitting the whole ionization kinetics at different concentrations with a double-channel rate $W_I(r)$ ($V_0 = 0.15$ eV, $V^* = 0.01$ eV, $S = 2.5$, $L = 1.24$ Å) and diffusion coefficient $D = 260$ Å^2/ns. (B) The same in the semilogarithmic scale showing the long time $N^*(t)$ asymptotes.

is still effective near the contact due to the lower activation barrier at $\lambda_c = 0.86$ eV. At larger distances, the role of the excited state channel becomes less prominent, and production of the ground state ion pairs prevails.

D. Fitting to the Diffusion-Accelerated Ionization. The microscopic parameters (eq 2.22) found in the previous section are relevant only to the initial (static) phase of the ionization. To describe the reaction at longer times, one has to account for the acceleration of the forward electron transfer by encounter diffusion of reactants. The only adjustable parameter of the diffusional operator, D, and the optimal value of L can be found by fitting the theory to the experimental data in the whole available time domain. The results of this fitting are shown in Figure 5, with the best fit parameters $D = 260$ Å^2 /ns $= 2.6 \times 10^{-5}$ cm^2/s and $L = 1.24$ Å.

Knowing all the rate parameters of ionization, we can now predict how it proceeds at any diffusion (Figure 6A). To inspect this prediction, one has to vary the solvent viscosity as it was

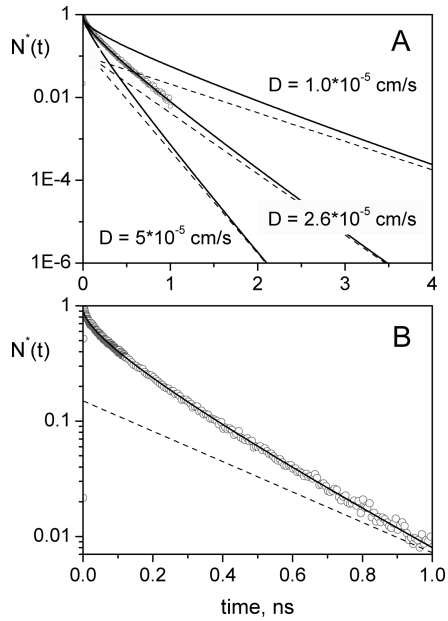

Figure 6. (A) Ionization kinetics at $c = 0.16$ M for the different encounter diffusions (solid lines) as well as their long time approximations (dashed lines). (B) The quality of this approximation to experimental data (○) is shown by a solid line while its exponential asymptote is indicated by a dashed line.

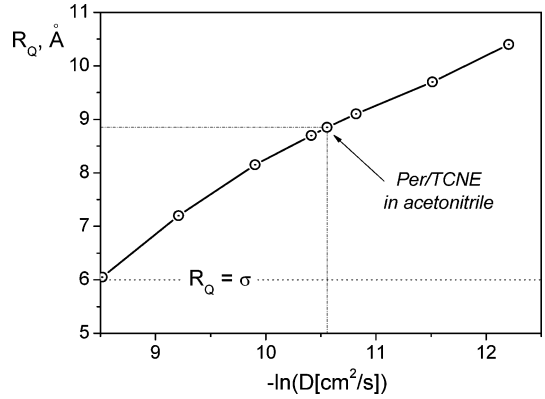

Figure 7. Diffusional dependence of the effective ionization radius R_Q. The R_Q value for the system under study is shown by the horizontal dash-dotted line.

done a few times for other systems.[4,5,19,20] The general form of the long time quenching kinetics obtained with DET, from eq 2.3 to eq 2.6, is well-known:[5,21]

$$\ln N = -t/\tau_D - c[4\pi R_Q D t + 8R_Q^2\sqrt{\pi D t}] \quad \text{at} \quad t \gg R_Q^2/D \tag{2.23}$$

At given D, this is a single-parameter expression, used a few times for fitting experimental data which are known in a restricted time interval after excitation.[5,22] In such a case, the nonstationary (transient) term $8R_Q^2(\pi D t)^{1/2}$ should be accounted for to get a correct R_Q value from the best fitting of the longest available time decay (Figure 6B). The proper R_Q can be extracted in the same way from the analytically available kinetic curves which are known for any D and t (Figure 6A). The corresponding $R_Q(D)$ dependence is shown in Figure 7. It is qualitatively the same as that found experimentally in ref : quasi-linear in ln (D) where the transfer is under diffusional control.

It is essential that, in the Per/TCNE system, $R_Q \approx 9$ Å is significantly larger then the contact distance $\sigma = 6$ Å where reaction is sensitive even to spherical anisotropy of the reactants. If the latter is pronounced, such a reaction may be pseudodiffusional provided it is contact (not remote). There is actually a number of such radical reactions subjected sometimes to special investigation reviewed in ref 23. But the electron transfer (unlike proton one) is hardly contact. As far as we know, there is only a single indication of such an opportunity when the kinetic reaction constant is affected by diffusion (probably by the rotational modulation of the stereospecific contact reaction).[24]

E. Double Channel versus Exponential Model. The system under study was recently subjected to an alternative interpretation based on arbitrary interpolation between the long-time asymptotes of static quenching ("in absence of reactants mobility") and that of the diffusional one which completes the excitation decay. Thus, the intermediate (transient) effect is lost as well as initial quasi-kinetic stage presented by eq 2.14. Instead, $N(t)$ diverges at $t \to 0$, so that neither classical Smoluchowski theory of contact quenching nor its Collins-Kimball modification is reproducible. The latter operates with a kinetic rate constant k_0 which is not specified in a "theory" of ref 25 as well as k_2.

Nonetheless, the authors reached a reasonable agreement of their theory with experimental data at large enough times assuming an exponential shape of a single-channel ionization rate

$$W(r) = \nu \exp(-2r/a) = W_c e^{-2((r-\sigma)/a)} \tag{2.24}$$

where a is the decay length analogous to our L. The reduction of a true ionization rate (eq 2.8) to its exponential approximation (eq 2.24) is only possible if one neglects DSE and the space dependence of $\lambda(r)$, setting $\tau = 0$ and $\lambda \equiv \lambda_c$. From fitting such a theory to the same data as in Figure 5, both its parameters, ν and a, were restored but not uniquely. There are two different sets of these parameters proposed in Table 4 of ref 25. Besides, they are different for all concentrations. Using some of them, we show a few variants of exponential rate by the straight lines in Figure 8. On the contrary, our double-channel rate 2.7 is presented there by a single curve for all concentrations as it should be.

It is clear from this comparison that the partial success of fitting reached in ref 25 should be attributed to the occasional proximity of our $W_I(r)$ to their exponents at $r \approx R_Q = 8.9$ Å, where the major diffusional quenching occurs. On the other hand, the slope of the straight lines is clearly smaller than that of a long tail of $W_I(r) \approx W_0(r)$ where it is actually $2/L$. As a result, the authors got $a = 2.8$ Å that was recognized to be "2−3 times larger than quantum chemistry estimations" which are in close agreement with our $L = 1.24$ Å obtained from the best fit.

Having $W_I(r)$ known, one can calculate from it the total kinetic constant of ionization k_0 and its partial values for each channel:

$$k_0 = \int W_0(r) d^3r + \int W^*(r) d^3r = k_0^0 + k_0^* \tag{2.25}$$

Their free energy dependencies are shown in Figure 9 in comparison with what was obtained for the rate constant of a single channel exponential ionization considered in ref 25. The latter is higher than our $k_0^0(\Delta G_i)$ which is hindered by DSE,

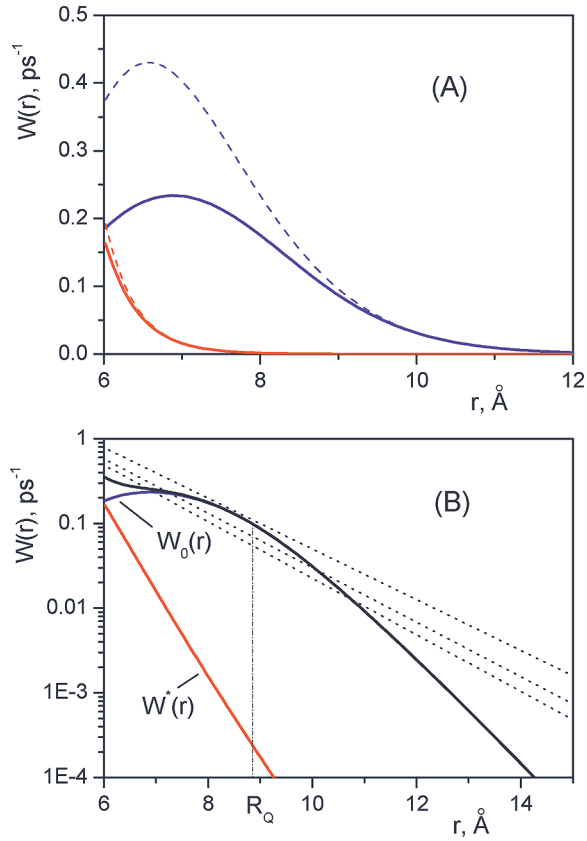

Figure 8. (A) Rates of the ion pairs production in their ground (blue) and excited (red) states with (solid) and without (dashed lines) account for DSE. (B) The total rate $W_I = W_0 + W^*$ (black line) and its components (blue and red) in comparison with a few straight dashed lines representing the exponential model 2.24 for some parameters given in ref 25.

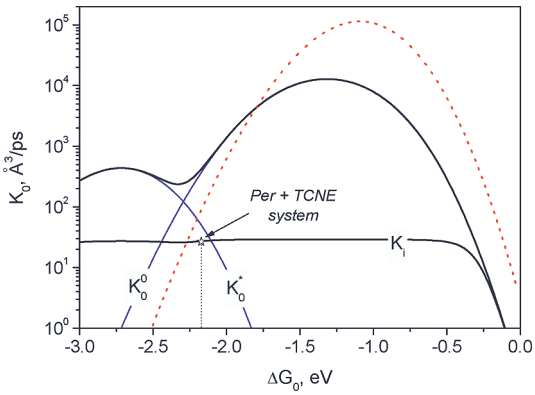

Figure 9. Free energy dependence of the kinetic rate constants for both channels, k_0^0 and k_0^* (blue lines), compared to that for the exponential model (red line). The true diffusional rate constant for diluted Per-TCNE system, $k_D = 4\pi R_Q D$, is shown by the star (*), indicating the height of the diffusional plateau in the Rehm−Weller plot.

and narrower than that which is broaden and shifted left because of $\lambda(r)$ dependence. However, the kinetic rate constant happens to be higher than the diffusional one in both approaches based on the same ionization kinetics obtained experimentally. This is one more confirmation that the point representing the system under study is truly located on the diffusional plateau of the Rehm−Weller plot, as was first stated in ref 26 (Figure 9).

Independent experimental evidence that ionization is under diffusional control is given by violation of the Stern−Volmer law obtained from the fluorescence quantum yield

$$\eta = \int_0^\infty \frac{N^*(t)}{N_0\tau_D}dt \equiv \int_0^\infty R(t)dt/\tau_D = \int_0^\infty N(t)dt/\tau_D = \frac{1}{1 + c\kappa\tau_D} \quad (2.26)$$

If the quenching of the fluorescence is under kinetic control

$$N(t) = e^{-t/\tau_D - ck_0 t} \text{ and } \frac{1}{\eta} = 1 + ck_0\tau_D$$

that is $\kappa \equiv k_0$ is concentration independent as in the original Stern−Volmer law where $1/\eta$ is linear in c. However, in general, eq 2.19 accounts for the transient effect via time dependent $k_I(t)$. As a result, $N(t)$ becomes nonexponential in time under diffusional control when the transient effect is most pronounced. In such a case, the linearity of the Stern−Volmer law is violated (Figure 10) because the corresponding $\kappa(c)$ is not a constant but monotonously increases with c, starting from the lowest diffusional value $\kappa(0) = k_D = 4\pi R_Q D$, as has been indicated in ref 6. The coincidence of the nonlinear concentration dependence of $1/\eta$ with the experimental data obtained, either from pulse or stationary measurements of η at any c, is an unambiguous confirmation of the perfect fitting of ionization controlled by encounter diffusion.

F. Initial Ion Distribution. Assuming that ions accumulated during ionization neither move nor recombine, we can calculate their distribution over starting distance. In fact, there are two of them, for ion pairs accumulated in their ground state, $m_0(r)$, and for those produced in the excited state, $m^*(r)$. According to the conventional theory,[1,9,10] they are

$$m_0(r) = W_0(r)\int_0^\infty n(r,t)N(t)dt, \quad m^*(r) = W^*(r)\int_0^\infty n(r,t)N(t)dt \quad (2.27)$$

and their total number is $m(r) = m_0(r) + m^*(r)$. The normalized total distribution shown in Figure 11 is just a sum of the partial ones:

$$f(r) = \frac{m(r)}{\int m(r)d^3r} = f_0(r) + f^*(r) \quad (2.28)$$

The excited radical ion pairs appear mainly at contact, being quasi-exponentially distributed around it. This is a privilege of the ions born in the normal Marcus region. On the contrary, the ground state pairs Per^+...$TCNE^-$ are produced in the inverted region, because of the larger exergonicity. They are known to have a bell-shaped distribution shifted out of contact.[1] It is seen from Figure 11 that at higher concentrations the contribution of the excited pairs grows and the contact density increases. This phenomenon facilitates the ion recombination that proceeds faster at contact.

III. Ion Pair Accumulation and Recombination

A. Initial Ion Accumulation. As follows from eq 2.18, the initial ion accumulation in kinetic regime proceeds linearly in time, with a slope

$$\dot{P} = ck_0 \quad (3.1)$$

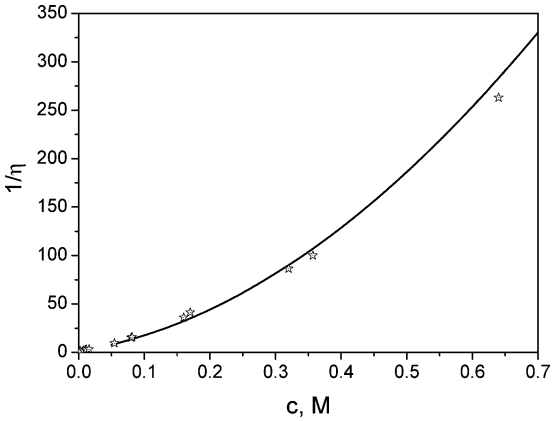

Figure 10. Concentration dependence of the theoretically calculated Stern−Volmer law (solid line) compared to that for the stationary fluorescence detected experimentally (points).

TABLE 2

c, M	0.16	0.32	0.64	0.90
A, ps^{-1}	0.091	0.162	0.149	0.186
γ	0.89	1.00	2.18	2.46

This linear time dependence is clearly seen in the experimental data: $P_{exp}(t) \simeq At$ for all of the measured ion kinetics at short times $t \in [0,\tau_L]$, where $\tau_L = 0.5$ ps is the time of dielectric relaxation in acetonitrile. The corresponding A values, extracted from the original experimental data at $c = 0.16$, 0.32, 0.64, and 0.9 M, are indicated in Table 2. Unlike ck_0 in eq 3.1, the four points $A(c)$ do not fall on a straight line with a slope $k_0 = 530$ Å^3/ps but are scattered around this line (see Figure 12).

The reasons of this discrepancy are not obvious and may be due to weaknesses of the present model. We however suggested here that indirect calibration[28] of the experimental $P_{exp}(t)$ for $c = 0.16$, 0.64, and 0.9 M may also be one of such reasons. One can suggest an alternative calibration that makes $\dot{P}(c)$ linear. Giving preference to the low concentration points (especially to $c = 0.32$ M used as the standard[28]), we eliminated the

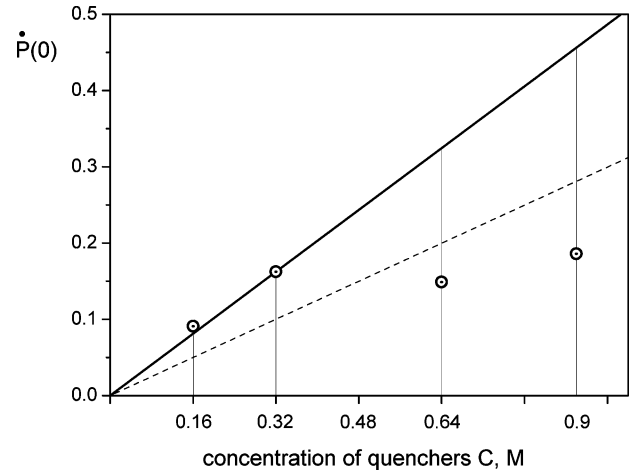

Figure 12. Initial rates of ion accumulation $\dot{P}_{exp} = A$ (⊙) compared to the expected linear dependence ck_0 (dashed line). The solid line with a higher slope $\tilde{k}_0$ (eq 3.2) represents the renormalized data linear in c.

scattering by multiplying the original experimental data on numerical factor γ:

$$P(t) = \gamma(c)P_{exp}(t) \tag{3.2}$$

These γ's (listed in Table 2) make $\dot{P}(0) = c\tilde{k}_0$ linear in c but with a higher ionization constant $\tilde{k}_0 = A(c)\gamma(c)/c = 842$ Å^3/ps $> k_0$ (solid line in Figure 12). If this is true, then there are more ions appearing at the very beginning than the excitations quenched during the same encounters.

In principle, such a situation is not impossible because our model ignores the straightforward light-induced transition $DA \rightarrow (D^*)^+ A^-$, as well as the radiative transitions $(D^*)^+ A^- \rightarrow D^+ A^-$. The very existence of such a circle explains why the total number of initially generated ions can exceed the number of the excitations quenched by ionization. Although there is a lack of experimental data related to this phenomenon, almost

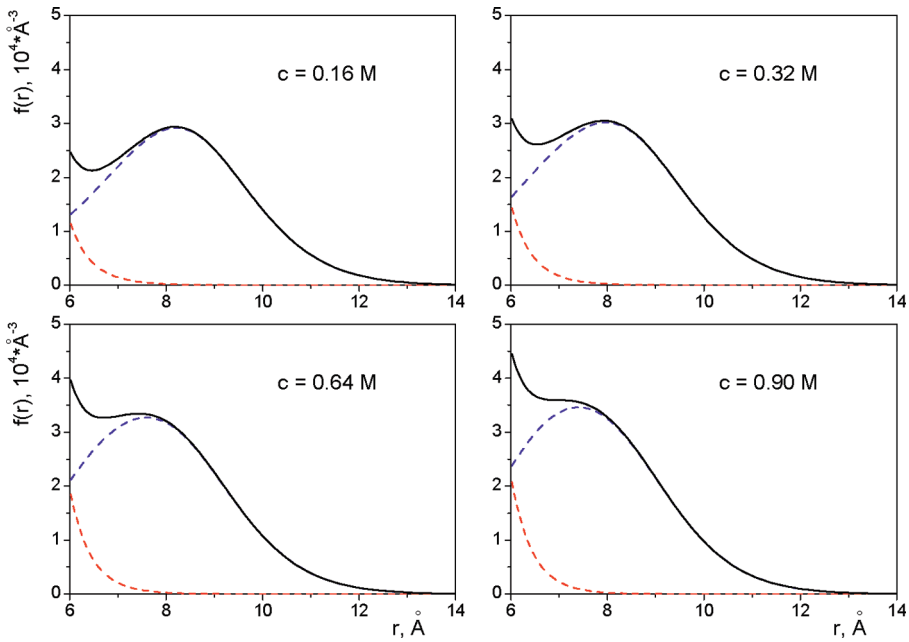

Figure 11. Solid lines: the normalized total density of ion pairs before recombination. Dashed lines: initial distributions of ions over charge separation in their ground (blue) and excited (red) states.

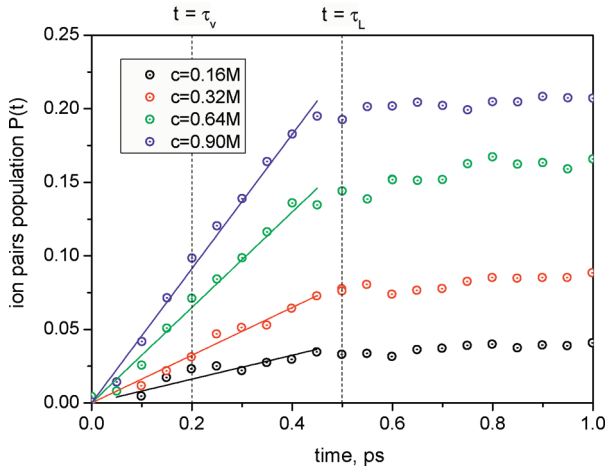

Figure 13. Renormalized kinetics of the initial ion pairs accumulation $P(t)$ at different concentrations of TCNE. The straight lines are the linear approximations of the initial kinetics (before recombination starts).

an exact frequency coincidence of light-absorbing transitions from DA to D^*A and $(D^*)^+A^-$ (Figure 1B) evidence in favor of this hypophysis.

In just the same way, one can correct the further time dependence of $P(t)$ by using eq 3.2 in the whole time domain available for $P_{exp}(t)$. The results shown in Figure 13 confirm that the initial linearity truly takes place for all concentrations though in a limited time interval, $t \leq \tau_L$. During this time, the system moving down from $q_1^{(n)}$ approaches the crossing points $q_R^{(n)}$ where recombination starts. This makes the subsequent accumulation slower, and after hot recombination, responsible for a sharp brake in $P(t)$, gives way to the final recombination of the thermalized ion pairs. The latter is the subject of the Unified Theory (UT).

B. Unified Theory. Extending the usual UT[1,9,10] to the case of a double-channel ionization, we have to introduce the densities of the ion pairs in their ground ($\mu(r,t)$) and excited states ($\mu^*(r,t)$), as well as that of the ground state product of recombination ($\pi(r,t)$). They obey the extended UT equations for irreversible recombination:

$$\frac{\partial \mu}{\partial t} = \alpha W_0(r) n(r,t) N(t) + \alpha^* W_R^*(r)\mu^* - W_R(r)\mu + \hat{\mathbf{L}}\mu \quad (3.3a)$$

$$\frac{\partial \mu^*}{\partial t} = W^*(r) n(r,t) N(t) - W_R^*(r)\mu^* + \hat{\mathbf{L}}\mu^* \quad (3.3b)$$

$$\frac{\partial \pi}{\partial t} = (1-\alpha) W_0(r) n(r,t) N(t) + (1-\alpha^*) W_R^*(r)\mu^* + W_R(r)\mu + D\Delta\pi \quad (3.3c)$$

Here the operator of encounter diffusion in the attractive Coulomb potential $U_c(r) = -r_c/r$ is

$$\hat{\mathbf{L}} = \frac{D}{r^2}\frac{\partial}{\partial r} r^2 e^{r_c/r} \frac{\partial}{\partial r} e^{-r_c/r}$$

where the Onsager radius $r_c = e^2/\varepsilon T$.

The rates of the ground state and excited ion pairs recombination are

$$W_R(r) = \sum_0^\infty \frac{U_R(r) e^{-S} S^n}{n! + U_R(r)\tau_0 e^{-S} S^n} \exp\left[-\frac{(\Delta G_R + \lambda + \hbar\omega n)^2}{4\lambda T}\right] \quad (3.4a)$$

$$W_R^*(r) = \sum_0^\infty \frac{U_R^*(r) e^{-S} S^n}{n! + U_R^*(r)\tau^* e^{-S} S^n} \exp\left[-\frac{(\Delta G_R^* + \lambda + \hbar\omega n)^2}{4\lambda T}\right] \quad (3.4b)$$

Here

$$\Delta G_R^* = \Delta G_R^*(\sigma) - T\left(\frac{r_c}{\sigma} - \frac{r_c}{r}\right), \qquad \Delta G_R = \Delta G_R(\sigma) - T\left(\frac{r_c}{\sigma} - \frac{r_c}{r}\right) \quad (3.5)$$

where

$$\Delta G_R^*(\sigma) = -\Delta E(\sigma) - \Delta G^*, \Delta G_R(\sigma) = -\Delta E(\sigma) - \Delta G_0$$

and

$$U_R(r) = \frac{V_R^2}{\hbar}\exp\left(-\frac{2(r-\sigma)}{L}\right)\frac{\sqrt{\pi}}{\sqrt{\lambda T}} \qquad U_R^*(r) = \frac{(V_R^*)^2}{\hbar}\exp\left(-\frac{2(r-\sigma)}{L}\right)\frac{\sqrt{\pi}}{\sqrt{\lambda T}} \quad (3.6)$$

The fractions of the initially created ions that survived hot recombination via two parallel reaction channels are $\alpha(r)$ and $\alpha^*(r)$, respectively. They determine the shape and share of final ion distributions, $\tilde{m}_0(r) = \mu(r,\infty)$ and $\tilde{m}^*(r) = \mu^*(r,\infty)$, preceding thermal recombination. To get them, one should integrate eqs 3.3a and 3.3a, setting $W_R = \hat{\mathbf{L}} = 0$:

$$\tilde{m}_0(r) = \alpha(r) W_0(r) \int_0^\infty n(r,t) N(t) dt = \alpha(r) \times m_0(r) \quad (3.7a)$$

$$\tilde{m}^*(r) = \alpha^*(r) W_R^*(r) \int_0^\infty \mu^*(r,t) dt = \alpha^*(r) \times m^*(r) \quad (3.7b)$$

They are smaller and different in shape than their precursors, $m_0(r)$ and $m^*(r)$.[8]

C. Hot Recombination. The fractions of the survived reactants in both channels were shown recently to be[8]

$$\alpha(r) = \prod_{n=0}^{n_{max}} (1 - Y_R^{(n)}) \quad \text{and} \quad \alpha^*(r) = 1 - \prod_{n=0}^{n_{max}} (1 - \tilde{Y}_I^{(n)}) \quad (3.8)$$

Here, $Y_R^{(n)}$ is the recombination probability for the ion pair, moving down along the D^+A^- surface, to recombine in points q_R^n (•), turning left and down to the DA state. Similarly, $\tilde{Y}_I^{(n)}$ is the ionization probability for a neutral pair moving down along the DA surface to turn right, to the ion pair ground state in the crossing points $\tilde{q}_I^{(n)}$ (degree; see Figure 1). These probabilities first obtained in ref 27 and used in our previous article[8] were defined as follows:

$$Y_R^{(n)} = \frac{2\pi V_{Rn}^2(r)}{|A_{1n}|}\left[1 + 2\pi V_{Rn}^2(r)\left(\frac{1}{|A_{1n}|} + \frac{1}{|A_{2n}|}\right)\right]^{-1} \tag{3.9a}$$

$$\tilde{Y}_I^{(n)} = \frac{2\pi V_{Rn}^2(r)}{|A_{2n}^*|}\left[1 + 2\pi V_{Rn}^2(r)\left(\frac{1}{|A_{2n}^*|} + \frac{1}{|A_{1n}^*|}\right)\right]^{-1} \tag{3.9b}$$

where

$$A_{1n} = \frac{q_R^{(n)} - 2\lambda}{\tau_L},\ A_{2n} = \frac{q_R^{(n)}}{\tau_L}$$

$$A_{1n}^* = \frac{\tilde{q}_I^{(n)} - 2\lambda}{\tau_L},\ A_{2n}^* = \frac{\tilde{q}_I^{(n)}}{\tau_L}$$

are the slopes of the levels in the crossing points. Being corrected in view of another λ_c, used in the present paper compared to the previous one, they were used for calculations of α and α^* together with a multiphonon coupling

$$V_{Rn}^2(r) = V_R^2(r)\frac{e^{-S_R}S_R^n}{n!} \tag{3.10}$$

From the best fit of the theory to the experimentally measured kinetics of ion accumulation and separation, the three varying microscopic parameters of recombination (V_R, V_R^*, and S_R) can be obtained, upon the assumption that the electronic tunnelling length $L_R = 1.24$ Å for recombination remains the same as that for the ionization reaction.

D. Fitting of the Thermalized Ions Recombination-Separation. As a matter of fact, the whole system 3.3 was solved numerically, but only accumulation and dissipation of the ground state ion pair population, $P(t) = \int[\mu(r,t) + \mu^*(r,t)]\mathrm{d}^3r/N_0$, detected experimentally, is available for fitting. At high concentrations, the theory essentially overestimates the survival probabilities of ions P_{exp} reported in the experimental work[28] as well as the free ion quantum yields $\phi = P_{exp}(\infty)$, that is the experimentally obtained plateau. However, the shape of the theoretical time dependence resembles the experimental one at any c and fits it well when P_{exp} is substituted for one, calibrated according to eq 3.2. The numerical multiplier γ (specified in Table 2) essentially shifts up the experimental curves for higher concentrations, up to their coincidence with the theoretical predictions.

The results of fitting the theory (solid lines) to the γ-corrected experimental data (degree) are shown in Figure 14. We failed to choose the unique values from the widely varying recombination parameters, but surprisingly a rather good fit was achieved with parameters identical to those for ionization:

$$S_R = 2.5,\ V_R = 0.15\ \mathrm{eV},\ V_R^* = 0.01\ \mathrm{eV} \tag{3.11}$$

The Onsager radius r_c was taken to be 14 Å, which agrees well with model estimations.

However, it remains unclear whether the present theory equally overestimates the number of ions before and after thermalization at high concentrations of TCNE or the photoconductivity method used in ref 29 underestimates this number, when the quencher concentration c is high as it is assumed here. The question is open for more detailed study of such a concentration phenomenon.

To make the physical picture more transparent, let us compare the distribution of ions survived in hot recombination, $\tilde{m}(r) = \tilde{m}_0(r) + \tilde{m}^*(r)$, with their initial distribution $m(r) = m_0(r) + m^*(r)$, as well as their total numbers before and after hot recombination:

$$\psi = \int m(r)d^3r = 1 - \eta \quad \text{and} \quad \tilde{\psi} = \int \tilde{m}(r)d^3r$$

As is seen from Figure 15, the hot recombination reduces the density of the survived ions near the contact where the backward electron transfer is more efficient. The total fraction of initially born ions, ψ, and what remains from it after hot recombination (thermalization), $\tilde{\psi}$, are listed in Table 3 together with the fluorescence quantum yield.

Roughly speaking 2/3 of the initially born ions are subjected to hot recombination and about 1/3 survive for subsequent thermal recombination, assisted by encounter diffusion.

E. Free Ions Bulk Recombination. After ions are separated, they continue to recombine in the bulk. The initial number of free ions participating in a bulk recombination is given by the height of the plateau reached by $N_\pm(t) = N_0P(t)$ at the end of the geminate stage. If the corresponding density of the free ions is $n_\pm(0) = N_\pm(1000\ \mathrm{ps})/V = (N_0/V)\phi$, then further on $n_\pm(t)$ decreases with time due to only bulk recombination:

$$\frac{1}{n_\pm(t)} = \frac{1}{n_\pm(0)} + k_Rt \tag{3.12}$$

where the rate constant of the homogeneous charge recombination is

$$k_R = \int W_R(r)\exp(r_c/r)d^3r \tag{3.13}$$

Here, $r_c = e^2/\varepsilon T$ is the Onsager radius, and $W_R(r)$ is the rate of thermal recombination via crossing points $q_R^{(n)}$ given in eq 3.4a. With the parameters listed in eq 3.11, it takes the form shown in Figure 16. Though the thermal recombination, proceeding in the normal Marcus region, decreases monotonously with ion separation, even this dependence is not exponential. One has to integrate it in eq 3.13 to get the theoretical estimate of

$$k_R = 1582\ \text{Å}^3/\mathrm{ps}$$

This prediction can be inspected experimentally by studying the bulk conductivity dissipation after photoionization.

IV. Conclusions

We launched here a new fitting for the experimental data on photoionization of perylene by tetracyanoethylene in acetonitrile solution, and the geminate recombination of ions, previously undertaken in refs 6 and 8. It is based on the corrected energy scheme (Figure 1) resulting from a direct estimation of the reorganization energy, λ_c, from the available spectroscopic data.

The new fit of the initial quasi-static ionization accounting for the vibrational relaxation and DSE provides us with reasonable limitations on the strength of the electronic tunnelling

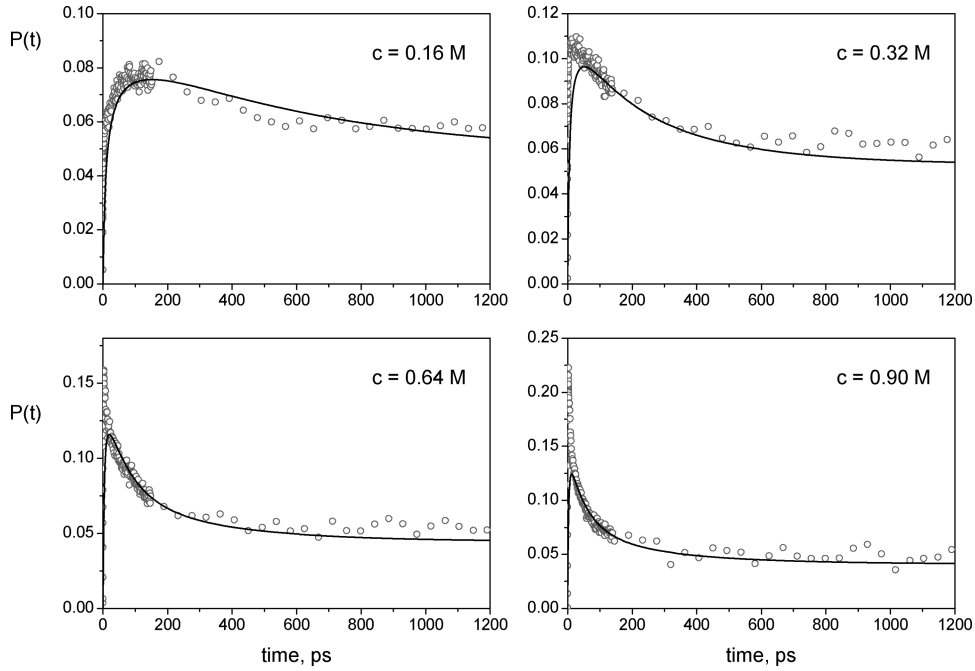

Figure 14. Ion accumulation-recombination kinetics data (degree) placed at our disposal by the authors of the experimental work[28] and calibrated by the factor $\gamma(c)$ (Table 2). They are fitted by the present theory with parameters listed in eq 3.11 (solid lines).

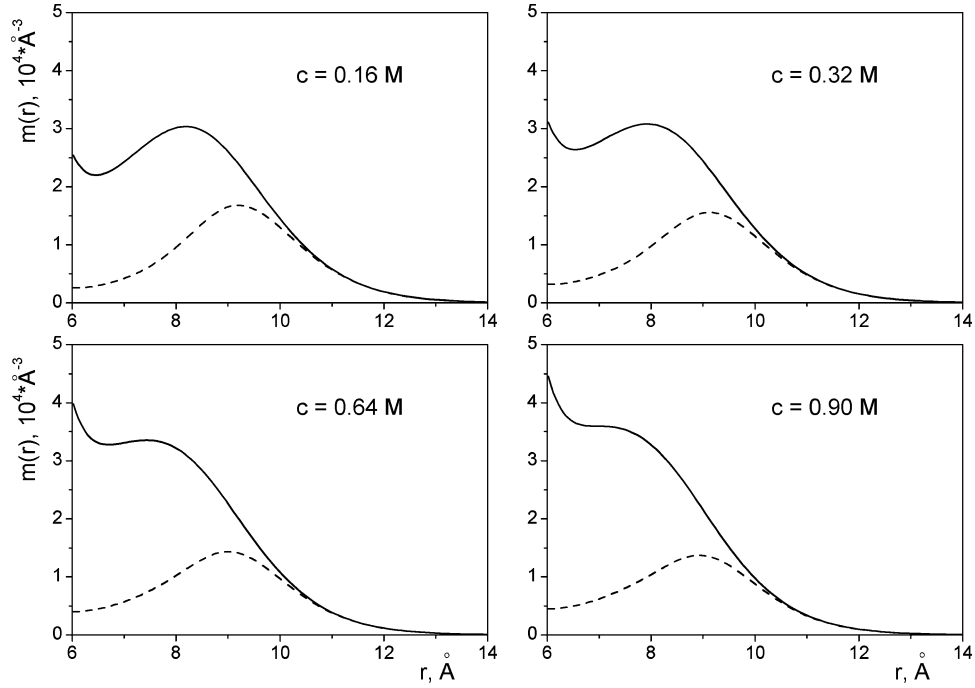

Figure 15. Initial distributions of ions $m(r)$ before thermalization (solid lines) and after it, $\tilde{m}(r)$ (dashed lines).

TABLE 3

TCNE concentration, c	0.16	0.32	0.64	0.9
Fluorescence quantum yield, η	0.031	0.011	0.003	0.002
Initial ionization yield, ψ	0.967	0.989	0.996	0.998
Yield of thermalized ions, $\tilde{\psi}$	0.372	0.366	0.328	0.312

resulting in either ground or excited state RIP production. The successful fitting of the subsequent diffusion-accelerated ionization eliminates uncertainties as to the contribution of the two competing channels and confirms that the forward electron transfer in the present system is under diffusional control. Moreover, the theory predicts what should be the quenching kinetics in solutions with other viscosities (different encounter diffusion). This conclusion can be inspected experimentally as well as the diffusional dependence of the quenching radius, $R_Q(D)$, presented in Figure 7.

The shapes of the two position-dependent ionization rates were specified, and their sum was compared with an alternative, exponential model of this quantity used in ref 25. The latter was shown to approximate the sum of the two rates in a limited range of distances near $r \approx R_Q$, but the model tunnelling length appears to be too large (2.8 Å) unlike our realistic value, $L =$ 1.24 Å. The free energy dependencies of the ionization rates are also different in the present and model theories, though both of them predict larger kinetic rate constants than the diffusional Stern−Volmer constant in the system under study. Thus, the diffusional nature of ionization is unambiguously established.

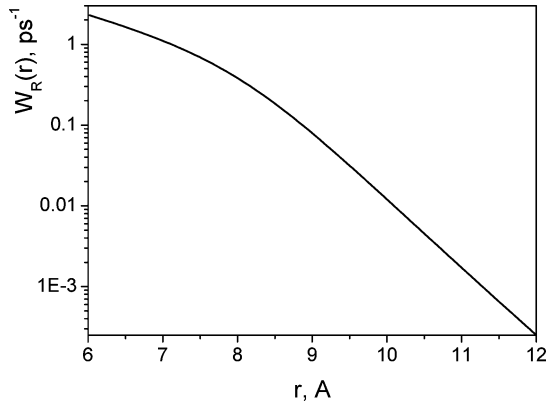

Figure 16. Nonexponential space dependence of ion recombination rate in the Marcus normal region.

The quasi-static ion accumulation preceding hot recombination is predicted to be linear in time, as it is actually. However, the slope of this linearity is scattered around the theoretical kinetic rate $\dot{P} = ck_0$. To eliminate this dispersion, it was assumed that the ionic population obtained experimentally, P_{exp}, should be corrected to restore the linearity in c, $P = \gamma(c)P_{exp}$. After such a correction, the subsequent hot recombination and the following thermal relaxation of survived RIPs were fitted well to the experimental data for four available concentrations. Using the obtained fitting parameters, we calculated the space distribution of ions before and after hot recombination and were convinced that only 1/3 of the initially created RIPs survive for subsequent thermal recombination. As to free ions which escape any geminate recombination, they continue to recombine in the bulk with a predicted rate constant k_R, which awaits experimental verification (Figure 13).

Acknowledgment. We are grateful to Professor E. Vauthey for placing at our disposal all of the experimental data we needed and to Professor A. I. Ivanov for continual interest in this work and for useful discussions. S.F. gratefully acknowledges the Weizmann Institute of Science and personally Professor S. Vega for the hospitality during his stay in Israel, as well as Russian Foundation for Basic Research for support (Grant 08-03-00534).

References and Notes

(1) Burshtein, A. I. *Adv. Chem. Phys.* **2000**, *114*, 419.
(2) Burshtein, A. I. *Adv. Chem. Phys.* **2004**, *129*, 105.
(3) Doktorov, A. B.; Burshtein, A. I. *Sov. Phys. JETP* **1975**, *41*, 671.
(4) Burshtein, A. I.; Kapinus, E. I.; Kucherova, I. Yu; Morozov, V. A. *J. Luminesc.* **1989**, *43*, 291.
(5) Gladkikh, V. S.; Burshtein, A. I.; Tavernier, H. L.; Fayer, M. D. *J. Phys. Chem. A* **2002**, *106*, 6982.
(6) Gladkikh, V.; Angulo, G.; Pagés, S.; Lang, B.; Vauthey, E. *J. Phys. Chem. A* **2004**, *108*, 6667.
(7) Pagés, S.; Lang, B.; Vauthey, E. *J. Phys. Chem. A* **2004**, *108*, 549.
(8) Gladkikh, V.; Burshtein, A. I.; Feskov, S. V.; Ivanov, A. I.; Vauthey, E. *JCP* **2005**, *123*, 244510.
(9) Burshtein, A. I. *Chem. Phys. Lett.* **1992**, *194*, 247.
(10) Dorfman, R. C.; Fayer, M. D. *J. Chem. Phys.* **1992**, *96*, 7410.
(11) Burshtein A. I. *Adv. Phys. Chem.*, doi: 10.1155/2009/214219.
(12) Marcus, R. A. *J. Chem. Phys.* **1956**, *24*, 966. *ibid* **43**, 679 (1965).
(13) Zusman, L. D. *Chem. Phys.* **1980**, *49*, 295.
(14) Yakobson, B. I.; Burshtein, A. I. *High. Energy. Chem.* **1981**, *14*, 211. (a) [KhVE **14** 291 (1980)].
(15) Zusman, L. D. *Zeit. Phys. Chem.* **1994**, *186*, 1–29.
(16) Rips, I.; Jortner, J. *J. Chem. Phys.* **1987**, *87*, 6513.
(17) Feskov, S.; Gladkikh, V.; Burshtein, A. I. *Chem. Phys. Lett.* **2007**, *447*, 162.
(18) Burshtein, A. I.; Kofman, A. G. *Chem. Phys.* **1979**, *40*, 289.
(19) Krissinel, E.; Burshtein, A. I.; Lukzen, N.; Steiner, U. *Mol. Phys.* **1999**, *96*, 1083.
(20) Angulo, G.; Grampp, G.; Neufeld, A. A.; Burshtein, A. I. *J. Phys. Chem. A* **2003**, *107*, 6913.
(21) Rice, S. A. In *Comprehensive Chemical Kinetics;* Elsiever: New York, 1985; issue *25*, p 404.
(22) Gladkikh, V. S.; Burshtein, A. I. *JCP* **2007**, *126*, 014506.
(23) Burshtein, A. I.; Khudyakov, I. V.; Yakobson, B. I. *Prog. React. Kinet.* **1984**, *13*, 221.
(24) Gladkikh, V.; Burshtein, A. I. *J. Chem. Phys.* **2007**, *126*, 014506.
(25) Kuzmin, M. G.; Soboleva, I. V.; Dolotova, E. V. *J. Phys. Chem. A* **2008**, *112*, 5131.
(26) Burshtein, A. I.; Ivanov, A. I. *Phys. Chem. Chem. Phys.* **2007**, *9*, 396.
(27) Ivanov, A. I.; Potovoi, V. V. *Chem. Phys.* **1999**, *247*, 245.
(28) Pages, S.; Lang, B.; Vauthey, E. *J. Phys. Chem. A* **2004**, *108*, 549.
(29) Henseler, A.; Vauthey, E. *J. Photochem. Photobiol. A* **1995**, *91*, 7.

JP901863T